Relative Location Estimation in Wireless Sensor Networks

Neal Patwari, Alfred O. Hero III, Matt Perkins, Neiyer S. Correal and Robert J. O'Dea

Abstract— Self-configuration in wireless sensor networks is a general class of estimation problems which we study via the Cramér-Rao bound (CRB). Specifically, we consider sensor location estimation when sensors measure received signal strength (RSS) or time-of-arrival (TOA) between themselves and neighboring sensors. A small fraction of sensors in the network have known location while the remaining locations must be estimated. We derive CRBs and maximum-likelihood estimators (MLEs) under Gaussian and log-normal models for the TOA and RSS measurements, respectively. An extensive TOA and RSS measurement campaign in an indoor office area illustrates MLE performance. Finally, relative location estimation algorithms are implemented in a wireless sensor network testbed and deployed in indoor and outdoor environments. The measurements and testbed experiments demonstrate 1 m RMS location errors using TOA, and 1 m to 2 m RMS location errors using RSS.

I. INTRODUCTION

In this paper, we consider location estimation in networks in which a small proportion of devices, called reference devices, have *a priori* information about their coordinates. We assume that all devices, regardless of their absolute coordinate knowledge, estimate the range between themselves and their neighboring devices. Such location estimation is termed 'relative location' because the range estimates collected are predominantly between pairs of devices of which neither has absolute coordinate knowledge. These devices without a priori information we call blind-folded devices. In cellular location estimation [1][2][3] and local positioning systems (LPS) [4][5], location estimates are made only using ranges between a blindfolded device and reference devices. Relative location estimation requires simultaneous estimation of multiple device coordinates, and enables greater accuracy as more devices are added into the network, even when new devices range to just a few close neighbors. Greater accuracy in the network is possible without increasing the burden of installation of more known-location reference devices.

Relative location systems require a network of devices capable of peer-to-peer range measurement, an ad-hoc networking protocol, and a distributed or centralized location estimation algorithm. Time-difference of arrival (TDOA)

measurements are not usually considered since ad-hoc devices aren't likely to be accurately synchronized. However, accurate two-way or 'round-trip' TOA ranging can been implemented using inquiry-response protocols [6][7]. Ranging is also possible using RSS, which is attractive from the point of view of device complexity and cost, but is traditionally seen as a coarse measure of range. In this article we will show that RSS can lead to accurate location estimates in dense sensor networks.

The recent literature has seen interest in location estimation algorithms for wireless sensor networks [8-14]. Distributed location algorithms offer the promise of solving multi-parameter optimization problems even with constrained resources at each sensor [8]. Devices can begin with local coordinate systems [9] and then iteratively repeat their location algorithm as neighbors estimate and broadcast more reliable and global location coordinates [10][11]. Distributed algorithms must be careful to assure convergence and to avoid 'error accumulation', in which errors propagate serially in the network. Centralized algorithms assume the application permits deployment of a central processor to perform the location estimation. In [12], device locations are resolved by convex optimization. Both [13] and [14] provide MLEs for sensor location estimation, when observations are angle-of-arrival and TOA [13] and when observations are RSS [14].

This article focuses on the accuracy possible using either TOA or RSS relative location estimation algorithms. The radio channel is notorious for its impairments [15][16], thus accurate sensor location is by no means a given. In wireless sensor networks "sensing data without knowing the sensor location is meaningless" [17]. The CRBs presented in this article provide a means to determine if the location accuracy necessary for a particular application is possible. We begin in Section II by considering CRBs for network self-calibration estimators. Next, we state the relative location estimation problem and derive CRBs and MLEs in Section III. Finally, we present extensive experimental results. In Section IV, measurements of TOA and RSS in a peer-to-peer network are used to provide an example of estimator performance. Real-time operation of relative location using RSS is demonstrated in Section V. Photos of the experiments, for best image quality, are included only in an electronic version of this article [18].

II. NETWORK ESTIMATION BOUNDS

In what we call network self-calibration problems, parameters of all devices in a network must be determined.

Neal Patwari and Alfred O. Hero III are with the University of Michigan, Dept. of EECS, Ann Arbor MI, USA. E-mail: [npatwari, hero]@eecs.umich.edu. Matt Perkins, Neiyer S. Correal, and Robert J. O'Dea are with Motorola Labs, Plantation, Florida, USA. E-mail: [M.Perkins, N.Correal, Bob.O'Dea]@Motorola.com. This material is based upon work supported by a NSF Graduate Research Fellowship.

Information comes both from measurements made between pairs of devices that indicate the relative parameters of the devices, and a subset of devices which know *a priori* their parameters. A network self-calibration estimator estimates the unknown device parameters. For example, distributed clock synchronization in a network could be achieved by devices observing pair-wise timing offsets when just a small number of devices are synchronous.

To formulate the estimation problem, consider device parameters $\boldsymbol{\theta}$. For simplicity, assume that each device has one parameter, that m reference devices have known parameters $\theta_{1-m} \ldots \theta_0$, and n blindfolded devices do not know their parameters $\theta_1 \ldots \theta_n$. Devices make pair-wise observations $X_{i,j}$ with density $f_{X|\boldsymbol{\theta}}(X_{i,j}|\theta_i, \theta_j)$. We allow for the case when devices make incomplete observations, since two devices may be out of range, or a limited channel may not allow the capacity needed for each pair of devices in the network to make observations. Specifically, let $H(i) \subseteq \{1-m, \ldots, n\}$ be the set of devices with which device i makes pair-wise observations. We assume that $i \notin H(i)$ since a device cannot make a pair-wise observation with itself. By symmetry, if $j \in H(i)$ then $i \in H(j)$.

We assume by reciprocity that $X_{i,j} = X_{j,i}$, thus it is adequate to consider only the lower triangle of the observation matrix $\mathbf{X}$ when formulating the joint likelihood function. In practice, if it is possible to make independent observations on the links from i to j, and from j to i, then we assume that a scalar sufficient statistic can be found. Finally, we assume $X_{i,j}$ are independent for $j < i$. Then the log of the joint conditional pdf is

$$l(\boldsymbol{\theta}) = \sum_{i=1-m}^{n} \sum_{\substack{j \in H(i) \\ j < i}} l_{i,j}, \quad \text{where } l_{i,j} = \log f_{X|\boldsymbol{\theta}}(X_{i,j}|\theta_i, \theta_j).$$

$$(1)$$

The Fisher information matrix (FIM) is defined as,

$$\mathbf{F} = -\mathrm{E}\nabla_{\boldsymbol{\theta}}(\nabla_{\boldsymbol{\theta}} l(\boldsymbol{\theta}))^T = \begin{bmatrix} f_{1,1} & \cdots & f_{1,n} \\ \vdots & \ddots & \vdots \\ f_{n,1} & \cdots & f_{n,n} \end{bmatrix} \quad (2)$$

As derived in Appendix A, the diagonal elements $f_{k,k}$ of $\mathbf{F}$ reduce to a single sum across $H(k)$, since there are $\#\{H(k)\}$ terms in (1) which depend on θ_k. The off-diagonal elements reduce further. When $k \neq l$, there is at most one term in (1) that is a function of both k and l.

$$f_{k,l} = \begin{cases} \sum_{j \in H(k)} \mathrm{E}\left[\frac{\partial^2}{\partial \theta_k^2} l_{kj}\right], & k = l \\ \mathrm{I}_{H(k)}(l)\mathrm{E}\left[\frac{\partial^2}{\partial \theta_k \partial \theta_l} l_{k,l}\right], & k \neq l \end{cases} \quad (3)$$

$\mathrm{I}_{H(k)}(l)$ is an indicator function, 1 if $l \in H(k)$ or 0 if not.

A. Conditions for a decreasing CRB

Intuitively, as more devices are used in the location estimator, the accuracy increases for all of the devices in the network. For an n device network, there are $O(n)$

parameters, but $O(n^2)$ ranges to use in their estimation. The analysis of this section proves that given certain conditions, the CRB decreases as devices are added to the network. Specifically, we compare the CRB for networks with n and $n+1$ blindfolded devices. For the n case, the FIM is $\mathbf{F}$ as given in (2), and for the $n+1$ case, define $\mathbf{G}$ to be the FIM.

Theorem 1: Let $[\mathbf{G}^{-1}]_{ul}$ be the upper left $n \times n$ block of $\mathbf{G}^{-1}$. If (1) $\frac{\partial}{\partial \theta_{n+1}} l_{k,n+1} = a\frac{\partial}{\partial \theta_k} l_{k,n+1}$ for some constant a not a function of X, $\forall k \in \{1 \ldots n\}$, and (2) device $n+1$ makes pair-wise observations between itself and at least one blindfolded device and at least two devices, in total; then two properties hold: (1) $\mathbf{F}^{-1} - [\mathbf{G}^{-1}]_{ul} \geq 0$ in the positive semi-definite sense, and (2) $\mathrm{tr}\,\mathbf{F}^{-1} > \mathrm{tr}\,[\mathbf{G}^{-1}]_{ul}$.

The proof of Theorem 1 is shown in Appendix B. The Gaussian and log-normal distributions in Section III will be shown to meet condition (1). Property (1) implies that the additional $(n+1)$st device does not impair the estimation of the original n parameters. Furthermore, property (2) implies that the sum of the CRB variance bounds for the n parameters strictly decreases when the conditions are met. Thus when a device enters a network and makes pair-wise observations with at least one blindfolded device and at least two devices in total, the bound on the average variance of the original n coordinate estimates is reduced. Note that properties (1) and (2) of Theorem 1 are trivially satisfied by the data processing theorem if the additional device does not increase the number of parameters.

In this analysis, blindfolded devices are not considered to be reference devices after their parameters have been estimated. Doing so would allow errors to accumulate as new blindfolded devices used inaccurate estimated parameters as reference to estimate their own parameters. However, future analysis might consider sub-optimal systems which estimate the accuracy of blindfolded device parameters and allow accurate devices to become references, thereby reducing the parameter space and complexity.

III. RELATIVE LOCATION ESTIMATION

In this section, we consider self-configuration problem of using RSS or TOA measurements between pairs of devices in a wireless network to estimate 2-D device location. Specifically, for a wireless sensor network of m reference and n blindfolded devices, The relative location problem is the estimation of $\theta = \{x_1, \ldots, x_n, y_1, \ldots, y_n\}$ given the known coordinates, $\{x_{1-m}, \ldots, x_0, y_{1-m}, \ldots, y_0\}$, and pairwise TOA or RSS measurements. In the TOA case, $T_{i,j}$ is the measured TOA between devices i and j in (s), and in the RSS case, $P_{i,j}$ is the measured received power between devices i and j in (mW). The assumptions of the general self-configuration problem still hold, ie. only a subset $H(k)$ of devices are in range of device k, $T_{i,j}$ and $P_{i,j}$ are taken to be upper triangular matrices, and measurements are independent.

We assume that $T_{i,j}$ is Gaussian distributed,

$$T_{i,j} \sim \mathcal{N}(d_{i,j}/c, \sigma_T^2), \quad d_{i,j} = \sqrt{(x_i - x_j)^2 + (y_i - y_j)^2}$$

$$(4)$$

where c is the speed of propagation, and σ_T^2 is not a function of $d_{i,j}$. We assume that $P_{i,j}$ is log-normal, thus the random variable $P_{i,j}(\text{dBm}) = 10 \log_{10} P_{i,j}$ is Gaussian,

$$
\begin{aligned}
P_{i,j}(\text{dBm}) &\sim \mathcal{N}(\bar{P}_{i,j}(\text{dBm}), \sigma_{dB}^2) \qquad (5) \\
\bar{P}_{ij}(\text{dBm}) &= P_0(\text{dBm}) - 10 n_p \log_{10}(d_{i,j}/d_0)
\end{aligned}
$$

where $P_{i,j}(\text{dBm})$ is the power in dBm received at device i transmitted by device j, $\bar{P}_{i,j}(\text{dBm})$ is the mean power in dBm, and σ_{dB}^2 is variance of the shadowing when expressed in dB. The mean received power is a function of $P_0(\text{dBm})$, the free-space received power in dBm at a reference distance d_0, the path loss exponent n_p, and the distance $d_{i,j}$. Typically, $d_0 = 1$m and P_0 is calculated from the free space path loss formula [19]. Thus n_p is the only parameter that is a function of the environment. For a particular types of environments, n_p may be known from prior measurements, or it could be left as a 'nuisance' parameter to estimate. In this paper, we derive the CRB assuming n_p is known, and future research might consider the effects of leaving n_p as a nuisance parameter.

Given (5), the density of $P_{i,j}$ is,

$$
f_{P|\boldsymbol{\theta}}(P_{i,j}|\boldsymbol{\theta}) = \frac{10/\log 10}{\sqrt{2\pi\sigma_{dB}^2}} \frac{1}{P_{i,j}} e^{-\frac{b}{8}\left(\log \frac{d_{i,j}^2}{\tilde{d}_{i,j}^2}\right)^2}
$$
$$
\text{where} \quad b = \left(\frac{10 n_p}{\sigma_{dB} \log 10}\right)^2, \quad \tilde{d}_{i,j} = d_0 \left(\frac{P_0}{P_{i,j}}\right)^{\frac{1}{n_p}}. \qquad (6)
$$

We have defined the distance $\tilde{d}_{i,j}$ to help see the physical meaning behind the measured power. It is actually the MLE of range $d_{i,j}$ given received power $P_{i,j}$.

Note that neither $P_{i,j}$ nor $T_{i,j}$ are assumed to be ergodic random variables – in fact, obstructions in the measured environment that result in shadowing and TOA errors do not usually change over time. The CRB gives a lower bound on the ensemble variance. If networks with the same device coordinates are implemented in many different areas, the variances of unbiased coordinate estimates are lower bounded by the CRB presented here.

The model assumptions made in this section will be shown to be valid in Section IV-A, using channel measurement and modeling literature and the data collected during the measurement campaign in Section IV. In the next sections, we first use the model assumptions to derive the CRB and MLE for both the RSS and TOA cases.

A. One-Dimensional TOA Example

As an example, consider using TOA measurements to locate devices that are limited to being located on a 1-D linear track. Assume all devices are in range of each other. This could be applied to location estimation on an assembly line. Consider m reference devices, and n blindfolded devices with coordinates $\boldsymbol{\theta} = \{x_1, \ldots, x_n\}$. The distribution of the observations is given by (4) with $d_{i,j} = |x_j - x_i|$. The 2nd partials of $l_{i,j}$ are, $\frac{\partial^2}{\partial x_j^2} l_{i,j} = -\frac{\partial^2}{\partial x_j \partial x_i} l_{i,j} = \frac{-1}{\sigma_T^2 c^2}$, which are constant w.r.t. the random variables $T_{i,j}$. Thus the FIM, calculated using (3), is

$\mathbf{F}_T = [(n+m)\mathbf{I}_n - 1]/(\sigma_T c)^2$, where $\mathbf{I}_n$ is the $n \times n$ identity matrix. For $m \geq 1$, the matrix is invertible, and

$$
\mathbf{F}_T^{-1} = \frac{\sigma_T^2 c^2}{m(n+m)} [m\mathbf{I}_n + 1].
$$

The variance bound of an unbiased estimator for x_i is,

$$
\sigma_{x_i}^2 \geq \sigma_T^2 c^2 \frac{m+1}{m(n+m)}. \qquad (7)
$$

The variance $\sigma_{x_i}^2$ is reduced more quickly by adding reference than blindfolded devices. However, for large m, the difference between increasing m and n is negligible. Intuitively for large m, the range information that blindfolded devices gain from an additional blindfolded device helps to more accurately locate them w.r.t. all m existing reference devices. This is almost as informative as being located w.r.t. an $(m+1)^{st}$ reference device.

B. Two-Dimensional Location Estimation

In the remainder of this article, 2-D location estimation is the focus. The 2-D unknown parameter vector is

$$
\boldsymbol{\theta} = \{x_1, \ldots, x_n, y_1, \ldots, y_n\}. \qquad (8)
$$

We call the FIMs for the RSS and TOA cases $\mathbf{F}_R$ and $\mathbf{F}_T$, respectively. Each device has two parameters, but (2) assumes that each device has only one. From the definition of the FIM in (2) we can see that the FIM for the 2-D case will have a similar form if partitioned into blocks,

$$
\mathbf{F}_R = \begin{bmatrix} \mathbf{F}_{Rxx} & \mathbf{F}_{Rxy} \\ \mathbf{F}_{Rxy}^T & \mathbf{F}_{Ryy} \end{bmatrix}, \quad \mathbf{F}_T = \begin{bmatrix} \mathbf{F}_{Txx} & \mathbf{F}_{Txy} \\ \mathbf{F}_{Txy}^T & \mathbf{F}_{Tyy} \end{bmatrix} \qquad (9)
$$

where the blocks $\mathbf{F}_{Rxx}$ and $\mathbf{F}_{Txx}$ are given by (3) using only the x parameter vector $\boldsymbol{\theta}_x = \{x_1, \ldots, x_n\}$, and the blocks $\mathbf{F}_{Ryy}$ and $\mathbf{F}_{Tyy}$ are given by (2) using only the y parameter vector $\boldsymbol{\theta}_y = \{y_1, \ldots, y_n\}$. The off-diagonal blocks $\mathbf{F}_{Rxy}$ and $\mathbf{F}_{Txy}$ have elements defined by,

$$
f_{k,l} = \begin{cases} \sum_{j \in H(k)} \text{E}\left(\frac{\partial l_{k,j}}{\partial x_k} \frac{\partial l_{k,j}}{\partial y_k}\right), & k = l \\ \text{I}_{H(k)}(l) E\left(\frac{\partial l_{k,l}}{\partial x_k} \frac{\partial l_{k,l}}{\partial y_l}\right), & k \neq l \end{cases}
$$

The elements of the sub-matrices of (9) are derived in Appendix C. For the RSS case, the elements are given by,

$$
\left[F_{Rxx}\right]_{k,l} = \begin{cases} b \sum_{i \in H(k)} \frac{(x_k - x_i)^2}{[(x_k - x_i)^2 + (y_k - y_i)^2]^2} & k = l \\ -b\, \text{I}_{H(k)}(l) \frac{(x_k - x_l)^2}{[(x_k - x_l)^2 + (y_k - y_l)^2]^2} & k \neq l \end{cases}
$$
$$
\left[F_{Rxy}\right]_{k,l} = \begin{cases} b \sum_{i \in H(k)} \frac{(x_k - x_i)(y_k - y_i)}{[(x_k - x_i)^2 + (y_k - y_i)^2]^2} & k = l \\ -b\, \text{I}_{H(k)}(l) \frac{(x_k - x_l)(y_k - y_l)}{[(x_k - x_l)^2 + (y_k - y_l)^2]^2} & k \neq l \end{cases}
$$
$$
\left[F_{Ryy}\right]_{k,l} = \begin{cases} b \sum_{i \in H(k)} \frac{(y_k - y_i)^2}{[(x_k - x_i)^2 + (y_k - y_i)^2]^2} & k = l \\ -b\, \text{I}_{H(k)}(l) \frac{(y_k - y_l)^2}{[(x_k - x_l)^2 + (y_k - y_l)^2]^2} & k \neq l \end{cases}
$$
$$
\qquad (10)
$$

For the TOA case, the elements are given by,

$$
\left[F_{Txx}\right]_{k,l} = \begin{cases} \frac{1}{c^2\sigma_T^2}\sum_{i\in H(k)} \frac{(x_k-x_i)^2}{(x_k-x_i)^2+(y_k-y_i)^2} & k=l \\ -\frac{1}{c^2\sigma_T^2}\mathrm{I}_{H(k)}(l)\frac{(x_k-x_l)^2}{(x_k-x_l)^2+(y_k-y_l)^2} & k\neq l \end{cases}
$$

$$
\left[F_{Txy}\right]_{k,l} = \begin{cases} \frac{1}{c^2\sigma_T^2}\sum_{i\in H(k)} \frac{(x_k-x_i)(y_k-y_i)}{(x_k-x_i)^2+(y_k-y_i)^2} & k=l \\ -\frac{1}{c^2\sigma_T^2}\mathrm{I}_{H(k)}(l)\frac{(x_k-x_l)(y_k-y_l)}{(x_k-x_l)^2+(y_k-y_l)^2} & k\neq l \end{cases}
$$

$$
\left[F_{Tyy}\right]_{k,l} = \begin{cases} \frac{1}{c^2\sigma_T^2}\sum_{i\in H(k)} \frac{(y_k-y_i)^2}{(x_k-x_i)^2+(y_k-y_i)^2} & k=l \\ -\frac{1}{c^2\sigma_T^2}\mathrm{I}_{H(k)}(l)\frac{(y_k-y_l)^2}{(x_k-x_l)^2+(y_k-y_l)^2} & k\neq l \end{cases} \quad (11)
$$

The CRBs for the RSS and TOA cases are $\mathbf{F}_R^{-1}$ and $\mathbf{F}_T^{-1}$, respectively. Note $\mathbf{F}_R \propto n_p/\sigma_{dB}$ while $\mathbf{F}_T \propto 1/(c^2\sigma_T^2)$. These SNR quantities directly affect the CRB. In the TOA case, the dependence on the coordinates is in unit-less distance ratios, indicating that the size of the system can be scaled without changing the CRB as long as the geometry is kept the same. However, in the RSS case, due to the d^4 terms in the denominator of each term of $\mathbf{F}_R$, the variance bound scales with the size of the system even if the geometry is kept the same. These scaling characteristics indicate that TOA will be preferred for sparse networks, but at some high density, RSS can perform as well as TOA.

Let $\hat{x}_i$ and $\hat{y}_i$ be unbiased estimators of x_i and y_i. We define the ith location estimate variance bound as

$$
\sigma_i^2 \leq \mathrm{Var}(\hat{x}_i) + \mathrm{Var}(\hat{y}_i).
$$

In general, σ_i^2 must be calculated via the inverse of the FIMs given above. However, for the one blindfolded device case, we present an analytical result.

C. Traditional Location System Example

Consider the network with blindfolded device 1 and reference devices $1-m\ldots 0$ which make pair-wise measurements with device 1. This example, with unknowns x_1 and y_1, is equivalent to many existing location systems, and a bound for the variance of the location estimator has been derived in the TOA case [2]. In the RSS case,

$$
E\left[(\hat{x}_1-x_1)^2+(\hat{y}_1-y_1)^2\right] \geq \sigma_1^2 = \frac{F_{Rxx}+F_{Ryy}}{F_{Rxx}F_{Ryy}-F_{Rxy}^2}
$$

from which we get the result that

$$
\sigma_1^2 = \frac{1}{b}\frac{\sum_{i=1-m}^0 d_{1,i}^{-2}}{\sum_{i=1-m}^{-1}\sum_{j=i+1}^0 \left(\frac{d_{1\perp i,j}d_{i,j}}{d_{1,i}^2 d_{1,j}^2}\right)^2}
$$

where the distance $d_{1\perp i,j}$ is the shortest distance from the point (x_1,y_1) to the line between device i and device j. For the TOA case, the result is,

$$
\sigma_1^2 = c^2\sigma_T^2 m\left[\sum_{i=1-m}^{-1}\sum_{j=i+1}^0 \left(\frac{d_{1\perp i,j}d_{i,j}}{d_{1,i}d_{1,j}}\right)^2\right]^{-1} \quad (12)
$$

The ratio $d_{1\perp i,j}d_{i,j}/(d_{1,i}d_{1,j})$ has been called the geometric conditioning $\mathcal{A}_{i,j}$ of device 1 w.r.t. references i and j [2]. $\mathcal{A}_{i,j}$ is the area of the parallelogram formed by the vectors from device 1 to i and from device 1 to j, normalized by the lengths of the two vectors. Thus the geometric dilution of precision (GDOP), defined as σ_1/σ_T, is

$$
GDOP = \sqrt{\frac{m}{\sum_{i=1-m}^{-1}\sum_{j=i+1}^0 \mathcal{A}_{i,j}^2}}
$$

which matches the result in [2]. The CRBs for the RSS and the TOA cases are shown in Fig. 1 when there are four reference devices located in the corners of a 1m by 1m square. The minimum of Fig. 1(a) is 0.27. Since the CRB scales with size in the RSS case, the standard deviation of location estimates in a traditional RSS system operating in a channel with $\sigma_{dB}/n_p = 1.7$ is limited to about 27% of the distance between reference devices. This performance has prevented use of RSS in many existing location systems and motivates the use of relative location information. Note in the TOA case, $\sigma_1 \propto c\sigma_T$, thus $c\sigma_T = 1$ was chosen in Fig. 1(b).
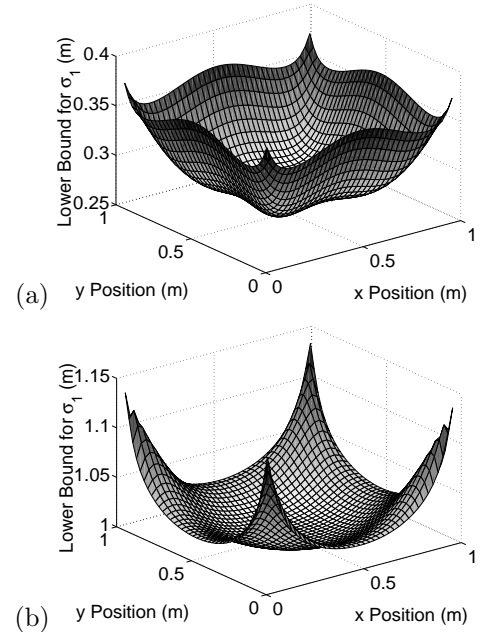

(a)

(b)

Fig. 1. σ_1 (m) for the example system vs. the coordinates of the single blindfolded device, for (a) RSS with $\sigma_{dB}/n = 1.7$, or (b) TOA with $c\,\sigma_T = 1$m.

D. Maximum Likelihood Relative Location Estimation

For the TOA case, the MLE of $\boldsymbol{\theta}$ is given by

$$
\hat{\boldsymbol{\theta}}_T = \arg\min \sum_{i=2-m}^n \sum_{\substack{j\in H(i)\\ j<i}} \left(c\,T_{i,j}-d_{i,j}\right)^2 \quad (13)
$$

The MLE for the 2-D RSS case is shown in [14] to be,

$$
\hat{\boldsymbol{\theta}}_{\tilde{R}} = \arg\min \sum_{i=2-m}^n \sum_{j\in H(i)} \left(\ln\frac{\tilde{d}_{i,j}^2}{d_{i,j}^2}\right)^2 \quad (14)
$$

Unlike in the TOA case, the RSS MLE is readily shown to be biased. Consider that for $n = 1$ and $m = 1$, the range between the two devices will be estimated to be equal to $\tilde{d}_{i,j}$. Using (6), the mean of $\tilde{d}_{i,j}$ is given by

$$E[\tilde{d}_{i,j}] = C\,d_{i,j}, \quad \text{where } C = e^{\frac{1}{2}\left(\frac{ln(10)}{10}\frac{\sigma_{dB}}{n_p}\right)^2}.$$

For typical channels, $C \approx 1.2$, adding 20% bias to the range. A bias-reduced MLE is preferred,

$$\hat{\boldsymbol{\theta}}_R = \arg\min \sum_{i=2-m}^{n} \sum_{j \in H(i)} \left(\ln \frac{\tilde{d}_{i,j}^2}{C^2 d_{i,j}^2}\right)^2 \qquad (15)$$

However, even with the reduction there is bias in the coordinate estimates. Consider $m = 4$ and $n = 1$. Place the reference devices at the corners of a 1 m by 1 m square and the blindfolded device within the square, the same as the case plotted in Fig. 1. We calculate via simulation [20] the bias gradient norm of $\hat{x}_1$ and display it in Fig. 2.

The gradient of the bias can be used in the uniform CRB to calculate the achievable variance of the biased estimator [20] as compared to all other estimators with same bias gradient norm. Fig. 2 shows that the bias gradient is high (with norm ≈ 1) at the corners of the square. Intuitively, (15) tries to force the ratio $\tilde{d}_{1,j}^2/(C^2 d_{1,j}^2)$ close to 1. When $\tilde{d}_{1,j}^2$ is small, the estimator has little freedom to place device 1 with respect to device j. In the limit as the actual locations of devices 1 and j become equal, the MLE will locate device 1 at device j with zero variance. Thus it makes sense that the simulated bias gradient norm is close to 1 at the corners of Fig. 2. Note that the bias of the MLE is close to zero near the center of the square. As a rule of thumb, the MLE has low bias for devices located near the center of their neighbors' positions.
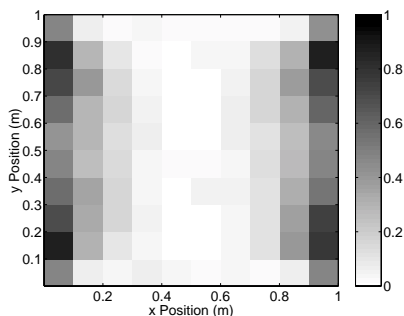

Fig. 2. Bias gradient norm of the RSS MLE of x_1 from (15) for the example system of Section III-C.

IV. Channel Measurement Experiment

In this section, we describe the measurement system and experiment and validate the channel model assumptions made at the start of Section III. A set of multipoint-to-multipoint (M2M) wideband channel measurements are conducted at the Motorola facility in Plantation, Florida. The measurement environment is a office area partitioned by 1.8m high cubicle walls, with hard partitioned offices, external glass windows and cement walls on the outside of the area. There are also metal and concrete support beams within and outside of the area. Offices are occupied with desks, bookcases, metal and wooden filing cabinets, computers and equipment. Forty-four device locations are identified within a 14m by 13m area and marked with tape.

The measurement system uses a wideband direct-sequence spread-spectrum (DS-SS) transmitter (TX) and receiver (RX) (Sigtek model ST-515). These measurements are one-way TOA measurements, that is, the RX does not reply to the TX. As discussed in Section I, devices in the two-way TOA case don't require synchronization since a round-trip delay can be measured at a single device. However, the one-way TOA measurements presented here require accurate synchronization. In this experiment, TX and RX are both triggered by a 1 pulse per second (1PPS) signal from two Datum ExacTime GPS and rubidium-based oscillators.

The TX and RX are battery-powered and are placed on carts. The TX outputs an unmodulated pseudo-noise (PN) code signal with a 40 MHz chip rate and code length 1024. The center frequency is 2443 MHz, and the transmit power is 10 mW. Both TX and RX use 2.4 GHz sleeve dipole antennas kept 1m above the floor. The antennas have an omnidirectional pattern in the horizontal plane and a measured antenna gain of 1.1 dBi. The RX records I and Q samples at a rate of 120 MHz, downconverts, and correlates them with the known PN signal and outputs a power-delay profile (PDP). We ensure that noise and ISM-band interference is not an issue by maintaining an SNR > 25 dB throughout the campaign.

The Datum oscillators at the TX and RX are carefully synchronized throughout each measurement day. After an initial GPS synch, GPS is disconnected and the rubidium oscillators provide stable 1PPS signals. The frequencies of the two rubidium oscillators are off very slightly, thus the 1PPS signals drift linearly, on the order of nanoseconds per hour. By periodically measuring and recording the offset between the two 1PPS signals using an oscilloscope, the effect of the linear drift can be cancelled. A time base with a standard deviation of approximately 1-2 ns is achieved. The uncertainty in the time base is thus a small source of error in the measured TOAs reported in Section IV-B.

The M2M measurements are conducted by first placing the TX at location 1 while the RX is moved and PDP measurements are made at locations 2 through 44. Then the TX is placed at location 2, as the RX is moved to locations 1 and 3 through 44. At each combination of TX and RX locations, the RX records five PDPs. All devices are in range of all other devices, so there are a total of 44*43*5 = 9460 measured PDPs. Since we expect reciprocity, there are a total of 10 PDPs for each link.

A. Estimating TOA and RSS

The wideband radio channel impulse response (CIR) is modeled as a sum of attenuated, phase-shifted, and time-delayed multipath impulses [16][19]. The PDP output of

the Sigtek measurement system, due to its finite bandwidth, replaces each impulse of the CIR with the autocorrelation function of the PN signal $R_{PN}(\tau)$, a triangular peak $2/R_C = 50ns$ wide. In high SNR, low multipath cases, TOA estimates can have better accuracy than $2/R_C$. However, a wider peak permits more multipath errors since the line-of-sight (LOS) component, with TOA $d_{i,j}/c$, can be obscured by non-LOS multipath that arrive $< 2/R_C$ after the LOS TOA. If the LOS component is attenuated, it can be difficult to distinquish the LOS TOA.

We estimate the LOS TOA by template-matching [21], in which samples of the leading edge of the PDP are compared to an oversampled template of $R_{PN}(\tau)$. The TOA estimate $\tilde{t}_{i,j}$ is the delay that minimizes the squared-error between the samples of the PDP and the template. Since non-LOS multipath are delayed in time, $\tilde{t}_{i,j}$ usually has a positive bias. We estimate the bias to be the average of $\tilde{t}_{i,j} - d_{i,j}/c$, $\forall i, j$ which in these measurements is 10.9 ns. In this paper we assume this bias is known for environments of interest, however, similar to n_p, this bias could be estimated as a 'nuisance' parameter. Subtracting out the bias from our measurements, we get the unbiased TOA estimator $t_{i,j}$. Finally, the average of the 10 $t_{i,j}$ measurements for the link between i and j we call $T_{i,j}$. The measured standard deviation, σ_T, is 6.1 ns.

It has been shown that a wideband estimate of received power, $p_{i,j}$, is obtained by summing the powers of the multipath in the PDP [19]. This wideband method reduces the frequency-selective fading effects. The geometric mean of the 10 $p_{i,j}$ measurements for the link between i and j, which we call $P_{i,j}$, reduces fading due to motion of objects in the channel. Shadowing effects, caused by permanent obstructions in the channel, remain predominant in $P_{i,j}$ since sensors are assumed to be stationary. Shadowing loss is often reported to be a log-normal random variable [22][16][19], which leads to the log-normal shadowing model in (5). As shown in Fig. 3, The measured $P_{i,j}$ match the log-normal shadowing model in (5) with $n = 2.30$ and $\sigma_{dB} = 3.92$ dB, using $d_0 = 1$m. The low variance may be due to the wide bandwidth, averaging, and the homogeneity of the measured cubicle area.

We experimentally verify the log-normal and Gaussian distributions of the RSS and TOA measurements by examining $P_{i,j}(\text{dBm}) - \bar{P}_{i,j}(\text{dBm})$ and $T_{i,j} - d_{i,j}/c$ via quantile-quantile plots in Fig. 4. RSS and TOA data fit the models well between the -2 and +2 quantiles, but the tails are heavier than the Gaussian distribution in the TOA case.

Finally, assuming i.i.d. measurements is somewhat oversimplified [23] but necessary for analysis. Using measurements remains important to verify true performance.

B. Measurement Results

Four devices near the corners are chosen as reference devices. The remaining 40 devices are blindfolded devices. The four reference device coordinates and either the RSS or TOA measurements, $P_{i,j}$ or $T_{i,j}$, are input to the MLE in (15) or (13). The minimum in each case is found via a conjugate gradient algorithm. The estimated device locations are compared to the actual locations in Fig. 5(a) and (b). To generalize the results, the RMS location error of all 40 unknown-location devices is 2.18m in the RSS case and 1.23m in the TOA case. Since shadowing and non-LOS errors are not ergodic, as discussed in Section IV-A, experimentally determining the MLE variances would require several measurement campaigns with the same device geometry but in different office areas. This was not possible due to resource and time limitations. Nevertheless, it is interesting to report the CRB for the measured network. We use the measured channel parameters, $\sigma_{dB}/n_p = 1.70$ and $\sigma_T = 6.1$ ns, the four reference devices used above, and the actual coordinates of all of the devices to calculate the FIMs in (10) for the RSS case and (11) for the TOA case. Taking the inverses of these two matrices, we have the CRBs. For the RSS and TOA cases, the quantity $\left(\sum_{i=1}^{40} \sigma_i^2 / 40 \right)^{1/2}$, is 0.76m and 0.69m, respectively.

We also notice that the devices close to the center are located more accurately than the devices on the edges, particularly in the RSS case. The MLE is seen not to suffer from error accumulation. Poor performance at the edges is expected since devices have fewer nearby neighbors to benefit their location estimate.
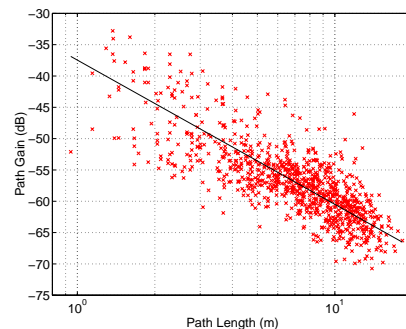

Fig. 3. Measured wideband path gain (x) as a function of path length. Linear fit (—) is with $d_0 = 1$m, $n_p = 2.3$, and $\sigma_{dB} = 3.92$.
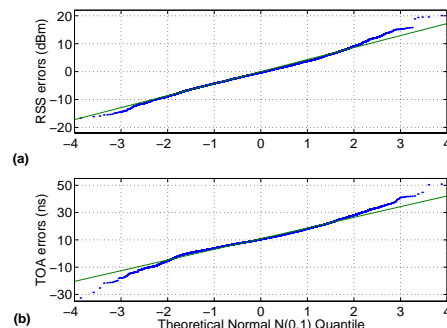

Fig. 4. Q-Q plot of sorted (a) measured dB shadowing errors $Z_{i,j}$ (dB), and (b) measured TOA estimation errors $\hat{T}_{i,j} - T_{i,j}$ (ns), compared to a standard Gaussian quantile.
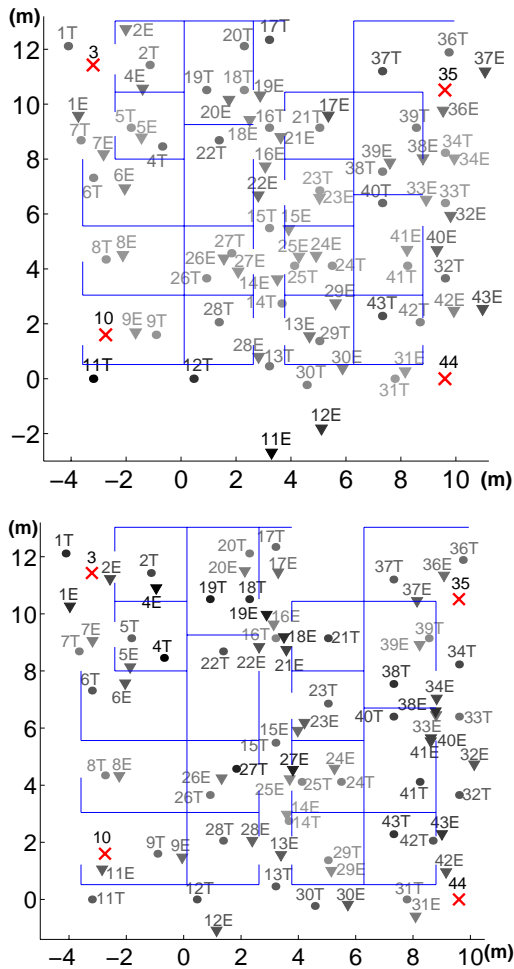
Fig. 5. True (●#T) and estimated (▼#E) location using (a) RSS and (b) TOA data for measured network with 4 reference devices (X#). Higher errors are indicated by darker text.

Fig. 6. True (●#T) and estimated (▼#E) location for the (a) parking lot and (b) residential home tests, using 4 reference devices (X#). Higher errors are indicated by darker text.

V. Testbed Experimentation

To provide an easy means for M2M radio channel measurement and location estimation tests, we developed and fabricated at Motorola Labs a testbed of 12 prototype peer-to-peer wireless sensor devices with RSS measurement capability. The devices have FSK transceivers with a 50 kHz data rate which operate in the 900-928 MHz band at one of 8 center frequencies separated by 4 MHz, which is approximately the coherence bandwidth of the channel. Devices slowly hop center frequencies so that RSS measurements can be taken at each f_c. While one device transmits, other devices measure its RSS. Packet transmissions are infrequent and packets are short, thus the channel is almost always silent. Devices are asynchronous and use a CSMA protocol. Thus RX measurements are not subject to multi-user interference. Every two seconds, each device creates a packet of measured RSS data and transmits it to a central 'listening' device, which uploads data to a laptop computer. The laptop has access to the known coordinates of the reference devices and the TX power and the RSS characteristic of the devices as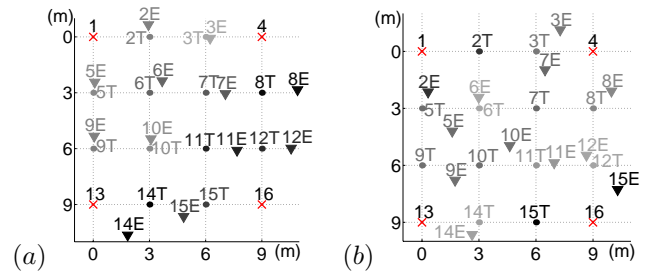 measured prior to deployment. The laptop stores the RSS for each pair of devices, each frequency that was measured, and each measurement over time.

First, we use the testbed as an easy way to estimate the path loss exponent n_p. When all of the device locations are known, the laptop uses the path loss vs. path length data to estimate the path loss exponent, n_p [24]. After estimating n_p, the blindfolded device coordinates are removed from the laptop and we operate the relative location estimation algorithm using the estimated n_p.

Then, the relative location estimation algorithm averages the measurements over time (using the most recent four RSS measurements), frequency (across 8 center frequencies), and the reciprocal channel. As presented in Section IV-A, log-normal shadowing remains predominant in the averaged measurement $P_{i,j}$. The maximum of the MLE in (15) is found using a conjugate gradient algorithm, which takes less than one second on the Pentium laptop. Each second an updated location is calculated and displayed on a map in a Visual Basic GUI. Real time tracking of slow movement (eg., walking) is possible.

A. Parking Lot Area

Testbed devices are placed in a 9 m by 9 m area in a 3 m grid in an empty area at the edge of the parking lot at the Motorola facility. The devices are kept at a height of 0.35 m. Using the testbed, we estimate n_p to be 3.2. Then, we place four reference devices at the corners of the area and place blindfolded devices at 7 of the remaining 12 spots in the grid (for 11 devices total). Devices record RSS and send packets as described above. The blindfolded devices are then moved to different positions in the grid for a new trial. 16 trials are run. The RMS location errors for the individual trials range from 0.9 m to 2.4 m. However, by moving 7 blindfolded devices around between positions, we record enough point-to-point ranges to see what would happen if there were 12 blindfolded devices, one in each spot on the grid. We use the recorded range data off-line to calculate that the RMS error would have been 1.46 m in this case. Furthermore, if we extended the duration of the time averaging from 4 ranges to 32 ranges, we would see the location estimates shown in Fig. 6(a), and we would reduce the RMS error to 1.02 m. Since shadow fading is not severe in this environment, time averaging is effective at improving location estimates.
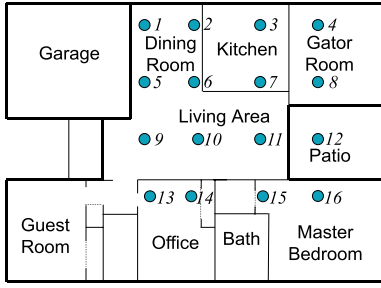
Fig. 7. Map of the grid of sensors in the Perkins home.

B. Residential Home

Next, we test the system in the Perkins home, a single-family, ranch-style house in Sunrise, Florida (Fig. 7). An identical 9 m by 9 m grid is used in this test, which spanned across many interior rooms and an outdoor patio. The obstructions include indoor walls, furnishings, appliances, and exterior walls & windows, and n_p is estimated using the testbed to be 4.0. Here, there are 4 reference devices in the corners of the grid and 8 other blindfolded devices. In 16 individual trials, the RMS location errors range from 1.0 m to 2.7 m. If all device ranges are used together, as described previously, we see the results in Fig. 6(b), in which the RMS error is 2.1 m. This error doesn't reduce significantly when the duration of time-averaging is increased from 4 to 32 ranges. The error is predominantly due to device #15, which has an error of 4.5 m. As shown in Fig. 7, device #15 is actually 3 m from device #14. However, significant shadowing is caused by the office closet and master bedroom closet that both lie directly in between the two devices $(P_{14,15}(\text{dBm}) - \bar{P}_{14,15}(\text{dBm}) = -22)$, and as a result the range estimate between the two is found to be 10.5 m. Unfortunately, this shadowing can't be countered by time or frequency averaging.

VI. CONCLUSIONS

The motivation of this article has been to show with what accuracy wireless sensor networks can estimate sensor locations. First, location estimation variance bounds in ad hoc networks are shown to decrease as more devices are added to the network. Next, CRBs can be readily calculated for arbitrary numbers and geometries of devices, and examples are presented. MLEs are presented and used in several real channels, both for TOA and RSS measurements. Sensor location estimation with about 1 m RMS error has been demonstrated using TOA measurements. However, despite the reputation of RSS as a coarse means to estimate range, it is also able to achieve an accuracy of about 1 m RMS in a testbed experiment. Fading outliers can still impair the RSS relative location system, implying the need for a robust estimator. Extension of this work to include 3-D location estimation will also be important in many applications. The results presented in this article should help wireless sensor network researchers determine if the accuracy possible from relative location estimation can meet their application requirements.

APPENDIX

A. CRB for Network Self-Calibration

The diagonal elements, $f_{k,k}$, of $\mathbf{F}$ given in (2) are,

$$f_{k,k} = \text{E}\left(\frac{\partial}{\partial \theta_k}l(X|\boldsymbol{\theta})\right)^2 = \text{E}\left(\sum_{j \in H(k)}\frac{\partial}{\partial \theta_k}l_{k,j}\right)^2$$

$$f_{k,k} = \sum_{j \in H(k)}\sum_{p \in H(k)}\text{E}\left(\frac{\partial}{\partial \theta_k}l_{k,j}\right)\left(\frac{\partial}{\partial \theta_k}l_{k,p}\right)$$

Since $X_{k,j}$ and $X_{k,p}$ are independent random variables, and $E[\frac{\partial}{\partial \theta_k}l_{k,j}] = 0$, the expectation of the product is only nonzero for $p = j$. Thus $f_{k,k}$ simplifies to the $k = l$ result in (3). The off-diagonal elements similarly simplify,

$$f_{k,l} = \sum_{j \in H(k)}\sum_{p \in H(l)}\text{E}\left(\frac{\partial}{\partial \theta_k}l_{k,j}\right)\left(\frac{\partial}{\partial \theta_l}l_{l,p}\right)$$

Here, due to independence and zero mean of the two terms, the expectation of the product will be zero unless both $p = k$ and $j = l$. Thus the $k \neq l$ result in (3).

B. Proof of Theorem 1

To prove Theorem 1, we compare $\mathbf{F}$, the FIM for the n device problem, to $\mathbf{G}$, the FIM for the $n + 1$ device case. Partition $\mathbf{G}$ into blocks,

$$\mathbf{G} = \begin{bmatrix} \mathbf{G}_{ul} & \mathbf{g}_{ur} \\ \mathbf{g}_{ll} & g_{lr} \end{bmatrix}$$

where $\mathbf{G}_{ul}$ is an $n \times n$ matrix, g_{lr} is the scalar Fisher information for the $n + 1$st parameter, and $\mathbf{g}_{ur} = \mathbf{g}_{ll}^T$ are $n \times 1$ vectors with kth element,

$$\mathbf{g}_{ur}(k) = \text{I}_{H(n+1)}(k)\,\text{E}\left(\frac{\partial}{\partial \theta_k}l_{k,n+1}\right)\left(\frac{\partial}{\partial \theta_{n+1}}l_{k,n+1}\right),$$

$$g_{lr} = \sum_{j \in H(n+1)}\text{E}\left(\frac{\partial}{\partial \theta_{n+1}}l_{n+1,j}\right)^2.$$

Let $l_n(X|\boldsymbol{\theta}_n)$ be the joint log-likelihood function in (1) for the n parameter case and $l_{n+1}(X|\boldsymbol{\theta}_{n+1})$ be the same function for the $n + 1$ parameter case, given by

$$l_{n+1}(X|\boldsymbol{\theta}_{n+1}) = \sum_{\substack{i = \\ 1-m}}^{n+1}\sum_{\substack{j \in H(i) \\ j < i}}l_{i,j} = l_n(X|\boldsymbol{\theta}_n) + \sum_{\substack{j \in \\ H(n+1)}}l_{n+1,j}.$$

Since $l_{n+1,j}$ is a function only of parameters θ_{n+1} and θ_j,

$$\frac{\partial^2}{\partial \theta_k \partial \theta_l}\sum_{\substack{j \in \\ H(n+1)}}l_{n+1,j} = \begin{cases} \text{I}_{H(n+1)}(k)\frac{\partial^2}{\partial \theta_k^2}l_{n+1,k}, & l = k \\ 0, & l \neq k \end{cases}$$

Thus $\mathbf{G}_{ul} = \mathbf{F} + \text{diag}(\mathbf{h})$, where $\mathbf{h} = \{h_1, \ldots, h_n\}$ and $h_k = \text{I}_{H(n+1)}(k)\text{E}(\frac{\partial}{\partial \theta_k}l_{n+1,k})^2$. Now, compare the CRB for the covariance matrix of the first n devices in the n and $n + 1$ blindfolded device cases, given by $\mathbf{F}^{-1}$ and $[\mathbf{G}^{-1}]_{ul}$,

respectively. Here, $[\mathbf{G}^{-1}]_{ul}$ is the upper left $n \times n$ submatrix of G^{-1},

$$[\mathbf{G}^{-1}]_{ul} = \left\{\mathbf{G}_{ul} - \mathbf{g}_{ur}g_{lr}^{-1}\mathbf{g}_{ll}\right\}^{-1} = \left\{\mathbf{F} + \mathbf{J}\right\}^{-1}$$
$$\text{where} \quad \mathbf{J} = \text{diag}(\mathbf{h}) - \frac{\mathbf{g}_{ur}\mathbf{g}_{ur}^T}{g_{lr}}$$

Both $\mathbf{F}$ and $\mathbf{J}$ are Hermitian. We know that $\mathbf{F}$ is positive semidefinite. Let $\lambda_k(\mathbf{F}), k = 1 \ldots n$ be the eigenvalues of $\mathbf{F}$ and $\lambda_k(\mathbf{F}+\mathbf{J}), k = 1 \ldots n$ be the eigenvalues of the sum, both listed in increasing order, then if we can show that $\mathbf{J}$ is positive semidefinite, then it is known [25] that:

$$0 \le \lambda_k(\mathbf{F}) \le \lambda_k(\mathbf{F} + \mathbf{J}), \forall k = 1 \ldots n \qquad (16)$$

Since the eigenvalues of a matrix inverse are the inverses of the eigenvalues of the matrix,

$$\lambda_k\left(\{\mathbf{F} + \mathbf{J}\}^{-1}\right) \le \lambda_k(\mathbf{F}^{-1}), \forall k = 1 \ldots n, \qquad (17)$$

which proves property 1 of Theorem 1. If in addition, we can show that $\text{tr}\mathbf{J} > 0$, then $\text{tr}\mathbf{F} + \mathbf{J} > \text{tr}\mathbf{F}$, and therefore $\sum_{k=1}^{n} \lambda_k(\mathbf{F} + \mathbf{J}) > \sum_{k=1}^{n} \lambda_k(\mathbf{F})$. This with (16) implies that $\lambda_j(\mathbf{F} + \mathbf{J}) > \lambda_j(\mathbf{F})$ for at least one $j \in 1 \ldots n$. Thus in addition to (17),

$$\lambda_j\left(\{\mathbf{F} + \mathbf{J}\}^{-1}\right) < \lambda_j(\mathbf{F}^{-1}), \text{for some } j \in 1 \ldots n$$

which implies that $\text{tr}\left(\{\mathbf{F} + \mathbf{J}\}^{-1}\right) < \text{tr}\mathbf{F}^{-1}$, which proves property 2 of Theorem 1.

1) Showing positive semidefiniteness and positive trace of $\mathbf{J}$: The diagonal elements of $\mathbf{J}$, $[\mathbf{J}]_{k,k}$ are,

$$[\mathbf{J}]_{k,k} = h_k - \frac{\mathbf{g}_{ur}^2(k)}{g_{lr}}.$$

If $k \notin H(n+1)$ then $h_k = 0$ and $\mathbf{g}_{ur}(k) = 0$, thus $[\mathbf{J}]_{k,k} = 0$. Otherwise, if $k \in H(n+1)$,

$$[\mathbf{J}]_{k,k} = \text{E}\left(\frac{\partial l_{n+1,k}}{\partial \theta_k}\right)^2 - \frac{\left[\text{E}\left(\frac{\partial l_{n+1,k}}{\partial \theta_k}\right)\left(\frac{\partial l_{n+1,k}}{\partial \theta_{n+1}}\right)\right]^2}{\sum_{j \in H(n+1)} \text{E}\left(\frac{\partial l_{n+1,j}}{\partial \theta_{n+1}}\right)^2}.$$

Because of the reciprocity assumption, the numerator of the fraction is equal to the square of the $j = k$ term in the sum in the denominator. Thus

$$[\mathbf{J}]_{k,k} \ge \text{E}\left(\frac{\partial}{\partial \theta_k} l_{n+1,k}\right)^2 - \text{E}\left(\frac{\partial l_{n+1,k}}{\partial \theta_k}\frac{\partial l_{n+1,k}}{\partial \theta_{n+1}}\right) = 0.$$

The equality will hold if k is the only member of the set $H(n+1)$. When condition (2) of Theorem 1 holds, $[\mathbf{J}]_{k,k}$ will be strictly greater than zero. Thus $\text{tr}\mathbf{J} > 0$.

Next, we show that $\mathbf{J}$ is diagonally dominant [25], i.e.,

$$[\mathbf{J}]_{k,k} \ge \sum_{\substack{j=1 \\ j \ne k}}^{n} |[\mathbf{J}]_{k,j}| = \sum_{\substack{j=1 \\ j \ne k}}^{n} \frac{|\mathbf{g}_{ll}(k)\mathbf{g}_{ll}(j)|}{g_{lr}},$$

where $[\mathbf{J}]_{k,k}$ is given in (18). Since $H(n+1) \ne \emptyset$, thus $g_{lr} > 0$, and an equivalent condition is,

$$g_{lr}h_k \ge |\mathbf{g}_{ll}(k)| \sum_{j=1}^{n} |\mathbf{g}_{ll}(j)|. \qquad (18)$$

If $k \notin H(n+1)$ then $h_k = 0$ and $\mathbf{g}_{ll}(k) = 0$, and the equality holds. If $k \in H(n+1)$, then

$$g_{lr}h_k = \text{E}\left(\frac{\partial l_{k,n+1}}{\partial \theta_k}\right)^2 \sum_{j \in H(n+1)} \text{E}\left(\frac{\partial l_{n+1,j}}{\partial \theta_{n+1}}\right)^2.$$

Because of condition (1) of Theorem 1,

$$\text{E}\left(\frac{\partial l_{k,n+1}}{\partial \theta_k}\right)^2 = \left|\text{E}\left(\frac{\partial l_{k,n+1}}{\partial \theta_{n+1}}\frac{\partial l_{k,n+1}}{\partial \theta_k}\right)\right|$$

Thus

$$g_{lr}h_k = |\mathbf{g}_{ll}(k)|\left[\sum_{\substack{j \ge 1 \\ j \in H(n+1)}} |\mathbf{g}_{ll}(j)| + \sum_{\substack{j \le 0 \\ j \in H(n+1)}} \left|\text{E}\left(\frac{\partial l_{j,n+1}}{\partial \theta_{n+1}}\frac{\partial l_{j,n+1}}{\partial \theta_j}\right)\right|\right]$$

Since $\mathbf{g}_{ll}(j) = 0$ if $j \notin H(n+1)$ we can include in the first sum all $j \in 1 \ldots n$. Since the 2nd sum is ≥ 0, (18) is true.

Diagonal dominance implies $\mathbf{J}$ is positive semidefinite, which proves (17). Note that if $H(n+1)$ includes ≥ 1 reference device, the 2nd sum is > 0 and the inequality in (18) is strictly > 0, which implies positive definiteness of $\mathbf{J}$ and assures that the CRB will strictly decrease.

C. CRB for Location Estimation

For the elements of $\mathbf{F}_R$, using (6) and (1),

$$l_{i,j} = \log\left(\frac{10\log 10}{\sqrt{2\pi\sigma_{dB}^2}}\frac{1}{P_{i,j}}\right) - \frac{b}{8}\left(\log\frac{d_{i,j}^2}{\hat{d}_{i,j}^2}\right)^2. \qquad (19)$$

Recall $d_{i,j} = \sqrt{(x_i - x_j)^2 + (y_i - y_j)^2}$. Thus,

$$\frac{\partial}{\partial x_j}l_{i,j} = -b\left(\log\frac{d_{i,j}^2}{\hat{d}_{i,j}^2}\right)\frac{x_j - x_i}{d_{i,j}^2}, \qquad (20)$$

Note that $\frac{\partial}{\partial x_j}l_{i,j} = -\frac{\partial}{\partial x_i}l_{i,j}$, thus the log-normal distribution of RSS measurements meets condition (1) of Theorem 1. The 2nd partials differ based on whether or not $i = j$ and if the partial is taken w.r.t. y_i or x_i. For example,

$$\frac{\partial^2 l_{i,j}}{\partial x_j \partial y_j} = -b\frac{(x_i - x_j)(y_i - y_j)}{d_{i,j}^4}\left[-\log\left(\frac{d_{i,j}^2}{\hat{d}_{i,j}^2}\right) + 1\right]$$
$$\frac{\partial^2 l_{i,j}}{\partial x_j \partial y_i} = -b\frac{(x_i - x_j)(y_i - y_j)}{d_{i,j}^4}\left[\log\left(\frac{d_{i,j}^2}{\hat{d}_{i,j}^2}\right) - 1\right] \quad (21)$$

All of the 2nd partials depend on the term, $\log(d_{i,j}^2/\hat{d}_{i,j}^2)$, which has an expected value of zero. The terms in (3) for each block of $\mathbf{F}_R$ in (9) simplify considerably and the final FIM takes the form in (10).

For the TOA case, the derivation is very similar, and the details are omitted for brevity.

REFERENCES

[1] P.-C. Chen, "A non-line-of-sight error mitigation algorithm in location estimation," in *IEEE Wireless Commun. and Netw. Conf.*, Sept. 1999, pp. 316–320.

[2] M. A. Spirito, "On the accuracy of cellular mobile station location estimation," *IEEE Trans. Veh. Technol.*, vol. 50, no. 3, pp. 674–685, May 2001.

[3] J. H. Reed, K. J. Krizman, B. D. Woerner, and T. S. Rappaport, "An overview of the challenges and progress in meeting the E-911 requirement for location service," *IEEE Commun. Mag.*, pp. 30–37, April 1998.

[4] J. Werb and C. Lanzl, "Designing a positioning system for finding things and people indoors," *IEEE Spectrum*, vol. 35, no. 9, pp. 71–78, Sept. 1998.

[5] A. Ward and A. H. A. Jones, "A new location technique for the active office," *IEEE Pers. Commun.*, vol. 4, no. 5, pp. 42–47, Oct. 1997.

[6] D. McCrady, L. Doyle, H. Forstrom, T. Dempsy, and M. Martorana, "Mobile ranging with low accuracy clocks," *IEEE Trans. Microwave Theory Tech.*, vol. 48, no. 6, pp. 951–957, June 2000.

[7] R. Fleming and C. Kushner, "Low-power, miniature, distributed position location and communication devices using ultra-wideband, nonsinusoidal communication technology," Aetherwire Inc., Semi-Annual Technical Report, ARPA Contract J-FBI-94-058, Tech. Rep., July 1995.

[8] A. Savvides, H. Park, and M. B. Srivastava, "The bits and flops of the n-hop multilateration primitive for node localization problems," in *Intl. Workshop on Sensor Nets. & Apps.*, Sept. 2002, pp. 112–121.

[9] S. Čapkun, M. Hamdi, and J.-P. Hubaux, "GPS-free positioning in mobile ad-hoc network," in 34th *IEEE Hawaii Int. Conf. on System Sciences (HICSS-34)*, Jan. 2001.

[10] J. Albowicz, A. Chen, and L. Zhang, "Recursive position estimation in sensor networks," in *IEEE Int. Conf. on Netw. Protocols*, Nov 2001, pp. 35–41.

[11] C. Savarese, J. M. Rabaey, and J. Beutel, "Locationing in distributed ad-hoc wireless sensor networks," in *ICASSP*, May 2001, pp. 2037–2040.

[12] L. Doherty, K. S. pister, and L. E. Ghaoui, "Convex position estimation in wireless sensor networks," in *IEEE INFOCOM*, vol. 3, 2001, pp. 1655 –1663.

[13] R. L. Moses, D. Krishnamurthy, and R. Patterson, "An auto-calibration method for unattended ground sensors," in *ICASSP*, vol. 3, May 2002, pp. 2941–2944.

[14] N. Patwari, R. J. O'Dea, and Y. Wang, "Relative location in wireless networks," in *IEEE VTC*, vol. 2, May 2001, pp. 1149–1153.

[15] K. Pahlavan, P. Krishnamurthy, and J. Beneat, "Wideband radio propagation modeling for indoor geolocation applications," *IEEE Commun. Mag.*, pp. 60–65, April 1998.

[16] H. Hashemi, "The indoor radio propagation channel," *Proc. IEEE*, vol. 81, no. 7, pp. 943–968, July 1993.

[17] J. M. Rabaey, M. J. Ammer, J. L. J. da Silva, D. Patel, and S. Roundy, "Picoradio supports ad hoc ultra-low power wireless networking," *IEEE Computer*, pp. 42–48, July 2000.

[18] A. O. Hero. Electronic version of this article. [Online]. Available: http://www.eecs.umich.edu/ hero/comm.html

[19] T. Rappaport, *Wireless Communications: Principles and Practice.* New Jersey: Prentice-Hall Inc., 1996.

[20] A. O. Hero, J. A. Fessler, and M. Usman, "Exploring estimator bias-variance tradeoffs using the uniform CR bound," *IEEE Trans. Signal Processing*, vol. 44, no. 8, pp. 2026–2041, Aug. 1996.

[21] B. B. Peterson, C. Kmiecik, R. Hartnett, P. M. Thompson, J. Mendoza, and H. Nguyen, "Spread spectrum indoor geolocation," *Journal of the Inst. of Navigation*, vol. 45, no. 2, pp. 97–102, Summer 1998.

[22] A. J. Coulson, A. G. Williamson, and R. G. Vaughan, "A statistical basis for lognormal shadowing effects in multipath fading channels," *IEEE Trans. Veh. Technol.*, vol. 46, no. 4, pp. 494–502, April 1998.

[23] N. Patwari, Y. Wang, and R. J. O'Dea, "The importance of the multipoint-to-multipoint indoor radio channel in ad hoc networks," in *IEEE Wireless Commun. and Netw. Conf.*, March 2002, pp. 608–612.

[24] G. Durgin, T. Rappaport, and H. Xu, "Measurements and models for radio path loss and penetration loss in and around homes and trees at 5.85 GHz," *IEEE J. Select. Areas Commun.*, vol. 46, no. 11, pp. 1484–1496, Nov. 1998.

[25] R. A. Horn and C. R. Johnson, *Matrix Analysis.* New York: Cambridge Univ. Press, 1990.